crystals

MDPI

Article

Magneto-Structural Correlation in μ-Hydroxo-μ-Carboxylato Hetero-Bridged Dinuclear Oxidovanadium(IV) Complexes

Ryo Yoshida, Masayuki Koikawa * and Tadashi Tokii

Department of Chemistry and Applied Chemistry, Faculty of Science and Engineering, Saga University, Honjo 1, Saga 840-8502, Japan
* Correspondence: koikawa@cc.saga-u.ac.jp

Abstract: Hetero-bridged dinuclear oxidovanadium(IV) complexes, $[(VO)_2\{HB(pz\}_3\}_2(\mu\text{-}OH)(\mu\text{-}O_2CR)]$ [R = C_2H_5, **1**; $(CH_3)_3C$, **2**; $(CH_3)_3CCH_2$, **3**; Ph_2CH, **4**; Ph_3C, **5**; $PhCH_2CH_2$, and **6**; $\{HB(pz)_3\}^-$ = hydrotris(pyrazolyl)borate], were synthesized and characterized using X-ray crystallography, infrared spectroscopy, UV-VIS spectroscopy, and elemental analysis. Structure analysis revealed that these complexes adopt a μ-hydroxo-μ-carboxylato hetero-bridged dinuclear structure. Magnetic measurements revealed ferromagnetic interactions ($J \sim +20$ cm^{-1}) between two V(IV) ions.

Keywords: dinuclear complex; oxidovanadium; crystal structure; hetero bridge; tripodal ligand; magnetic property

1. Introduction

Vanadium chemistry has attracted considerable attention due to its catalytic properties [1–3], ability to assemble into clusters [4–6], and roles in biological processes [7–9]. In magnetochemistry, oxidovanadium(IV) complexes, with their $S = 1/2$ spin state, are analogous to copper(II) complexes and are considered suitable for fundamental studies of magnetic interactions between metal centers. However, unlike copper(II) ions, oxidovanadium(IV) complexes have different magnetic orbitals, and superexchange interactions through bridging groups are generally weaker. This has led to slower progress in research on oxidovanadium(IV) complexes compared to dinuclear copper(II) complexes. Since around 1990, reports of dinuclear oxidovanadium(IV) complexes bridged by monoatomic ligands such as bis-μ-hydroxo or bis-μ-alkoxo groups increased significantly [10–20]. In these complexes, superexchange interactions through such bridging groups are expected to be minimal; however, some of these complexes exhibit strong antiferromagnetic interactions. Furthermore, the strength of these interactions has been found to vary depending on factors such as the vanadium–vanadium distance, the bond angles of the bridging atoms, and the dihedral angles of the equatorial planes surrounding the vanadium ions. These findings led to systematic investigations of direct interactions between vanadium d_{xy} orbitals and magneto-structural correlations, focusing on the geometric structures of the vanadium ions and the bridging configurations in binuclear planes [21–26].

In contrast, diatomic-bridged complexes, such as bis-μ-carboxylato bridges, typically exhibit longer V···V distances (>4 Å) and non-planar dinuclear planes defined by two V=O equatorial planes. As a result, even direct interactions between d_{xy} orbitals are expected to be minimal. However, a strong antiferromagnetic interaction ($J = -114$ cm^{-1}) has been reported for $[(VO)(tmtacn)(O_2CCH_3)]_2I_2$ (tmtacn = 1,4,7-trimethyl-1,4,7-triazacyclononane) [19], suggesting the potential for superexchange interactions through μ-carboxylato bridges. Furthermore, a hetero-bridged oxidovanadium(IV) complex, $[(VO)_2\{HB(pz)_3\}_2(OH)(O_2CCH_3)]$, featuring both monoatomic and diatomic bridges, has been shown to exhibit a ferromagnetic interaction [18]. To comprehensively understand these magnetic properties, it is essential to systematically investigate magneto-structural correlations, particularly by increasing the number of examples of diatomic-bridged and hetero-bridged oxidovanadium(IV) complexes.

check for updates

Citation: Yoshida, R.; Koikawa, M.; Tokii, T. Magneto-Structural Correlation in μ-Hydroxo-μ-Carboxylato Hetero-Bridged Dinuclear Oxidovanadium(IV) Complexes. *Crystals* **2024**, *14*, 1072. https://doi.org/10.3390/cryst14121072

Academic Editor: Jiayi He

Received: 27 November 2024
Revised: 9 December 2024
Accepted: 11 December 2024
Published: 12 December 2024

Copyright: © 2024 by the authors. Licensee MDPI, Basel, Switzerland. This article is an open access article distributed under the terms and conditions of the Creative Commons Attribution (CC BY) license (https://creativecommons.org/licenses/by/4.0/).

In this study, we synthesized six new μ-hydroxo-μ-carboxylato dinuclear oxidovanadium(IV) complexes, $[(VO)_2\{HB(pz)_3\}_2(\mu\text{-}OH)(\mu\text{-}O_2CR)]$ [R = C_2H_5, **1;** $(CH_3)_3C$, **2**; $(CH_3)_3CCH_2$, **3**; Ph_2CH, **4**; Ph_3C, **5**; $PhCH_2CH_2$, and **6**; $\{HB(pz)_3\}^-$ = hydrotris(pyrazolyl)borate] (Figure 1). Their crystal structures and magnetic properties were characterized, and the factors underlying ferromagnetic interactions and magneto-structural correlations in these hetero-bridged binuclear complexes were systematically investigated.

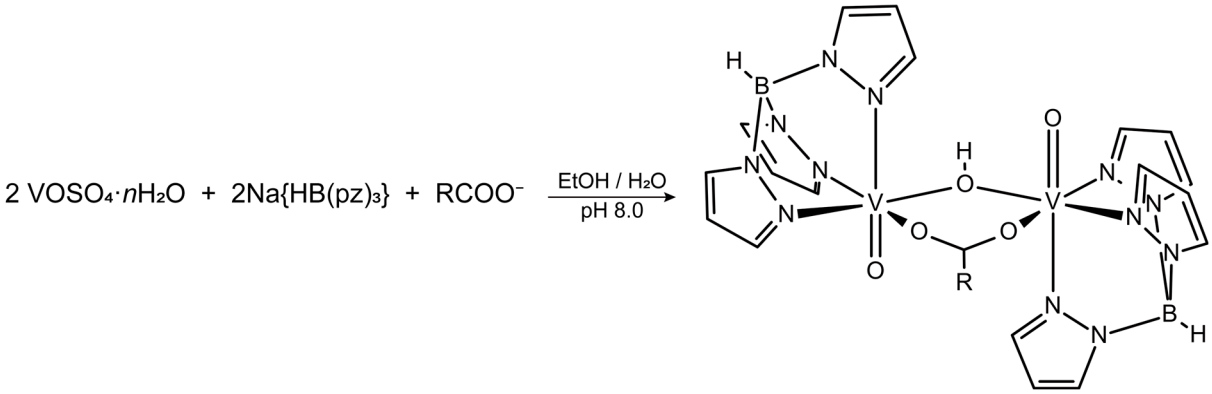


Figure 1. Reaction scheme for $[(VO)_2\{HB(pz)_3\}_2(\mu\text{-}OH)(\mu\text{-}O_2CR)]$.

2. Materials and Methods

2.1. Preparation

All chemicals were used as received unless otherwise noted. Ethanol was purified by distillation over magnesium turnings. Sodium hydrotris(pyrazolyl)borate $[NaHB(pz)_3]$ was synthesized according to a literature method [27,28].

2.1.1. $[(VO)_2\{HB(pz)_3\}_2(\mu\text{-}OH)(\mu\text{-}O_2CH_2CH_3)]$ (1)

Vanadium(IV) oxide sulfate *n*-hydrate (0.205 g, 1.23 mmol) was dissolved in 20 mL of an ethanol–water (9:1) mixture. Sodium hydrotris(pyrazolyl)borate (0.281 g, 1.19 mmol) was then added, and the mixture was stirred for 1 h. After filtration of the resulting white precipitate, sodium propionate (0.204 g, 2.08 mmol) was added, and the mixture was stirred for an additional day. Purple single crystals suitable for X-ray analysis were obtained. **1**·2EtOH; Yield: 0.284 g, 62.1%. Anal. Calc. for $C_{25}H_{38}B_2N_{12}O_7V_2$: C, 40.46; H, 5.16; N, 22.65, V, 13.73%. Found: C, 40.64; H, 5.11; N, 22.70; V, 13.59%. IR (ATR) [cm^{-1}]: 3622(vw), 3117(vw), 2485(vw), 1734(vw), 1541(s), 1504(m), 1405(s), 1307(s), 1211(s), 1116(m), 1046(s), 967(vs), 763(s), 714(vs), 661(s), 620(m), 551(m), 450(w).

2.1.2. $[(VO)_2\{HB(pz)_3\}_2(\mu\text{-}OH)(\mu\text{-}O_2C\text{-}t\text{-}Bu)]$ (2)

Vanadium(IV) oxide sulfate *n*-hydrate (0.210 g, 1.26 mmol) was dissolved in 20 mL of an ethanol–water (9:1) mixture. Sodium hydrotris(pyrazolyl)borate (0.288 g, 1.24 mmol) was added, and the mixture was stirred for 1 h. After filtration of the resulting white precipitate, pivalic acid (0.200 g, 2.07 mmol) was added, and the pH was adjusted to 8 using triethylamine. The mixture was stirred for 1 day, yielding purple single crystals suitable for X-ray analysis. **2**; Yield: 0.269 g, 41.6%. Anal. Calc. for $C_{23}H_{30}B_2N_{12}O_5V_2$: C, 40.74; H, 4.46; N, 24.79; V, 15.03%. Found: C, 40.81; H, 4.50; N, 24.79; V, 15.86%. IR (ATR) [cm^{-1}]: 3626(vw), 3115(vw), 2471(vw), 1517(s), 1420(m), 1406(s), 1308(s), 1213(s), 1115(m), 1044(s), 969(vs), 7563(s), 715(vs), 661(s), 619(m), 555(m), 461(m).

2.1.3. $[(VO)_2\{HB(pz)_3\}_2(\mu\text{-}OH)(\mu\text{-}O_2CCH_2\text{-}t\text{-}Bu)]$ (3)

Complex **3** was obtained as purple powder using the same method as **2**, with 3,3-dimethylbutanoic acid as the bridging carboxylate. Single crystals suitable for X-ray analysis were obtained by recrystallization from dichloromethane. **3**; Yield: 0.271 g, 65.3%. Anal. Calc. for $C_{24}H_{32}B_2N_{12}O_5V_2$: C, 41.65; H, 4.66; N, 24.29; V, 14.72%. Found: C, 41.74;

H, 4.57; N, 24.38; V, 15.32%. IR (ATR) [cm^{-1}]: 3627(vw), 3117(vw), 2472(vw), 1710(vw), 1522(m), 1504(m), 1405(s), 1308(s), 1211(s), 1115(m), 1044(s), 970(vs), 935(m), 755(s), 714(vs), 661(m), 619(m), 554(m), 462(w).

2.1.4. $[(VO)_2\{HB(pz)_3\}_2(\mu\text{-}OH)(\mu\text{-}O_2CCHPh_2)]$ (4)

Complex **4** was obtained as purple single crystals using the same method as **3**, with diphenylacetic acid as the bridging carboxylate. **4**; Yield: 0.315 g, 57.7%. Anal. Calc. for $C_{32}H_{33}B_2N_{12}O_5V_2$: C, 48.76; H, 4.09; N, 21.33; V, 12.93%. Found: C, 48.83; H, 4.12; N, 21.12; V, 13.29%. IR (ATR) [cm^{-1}]: 3643(vw), 3110(vw), 2476(vw), 1522(s), 1503(m), 1404(s), 1307(m), 1211(m), 1114(m), 1048(s), 967(vs), 931(m), 755(s), 714(vs), 660(m), 621(m), 557(m), 453(w).

2.1.5. $[(VO)_2\{HB(pz)_3\}_2(\mu\text{-}OH)(\mu\text{-}O_2CCPh_3)]$ (5)

Complex **5** was obtained as purple single crystals using the same method as **2**, with triphenylacetic acid as the bridging carboxylate. **5**·EtOH; Yield: 0.271 g, 65.3%. Anal. Calc. for $C_{40}H_{42}B_2N_{12}O_6V_2$: C, 52.77; H, 4.65; N, 18.46 V, 11.19%. Found: C, 53.16; H, 4.39; N, 18.34; V, 11.58%. IR (ATR) [cm^{-1}]: 3633(vw), 3106(vw), 2465(vw), 1750(vw), 1586(s), 1527(w), 1425(w), 1404(s), 1306(s), 1209(s), 1114(s), 1044(s), 968(vs), 935(m), 755(s), 714(vs), 661(m), 621(m), 599(w), 567(m), 492(s).

2.1.6. $[(VO)_2\{HB(pz)_3\}_2(\mu\text{-}OH)(\mu\text{-}O_2CCH_2CH_2Ph)]$ (6)

Complex **6** was obtained as purple single crystals using the same method as **3**, with 3-phenylpropionic acid as the bridging carboxylate. **6**; Yield: 0.246 g, 55.4%. Anal. Calc. for $C_{27}H_{30}B_2N_{12}O_5V_2$: C, 44.66; H, 4.16; N, 23.15 V, 14.03%. Found: C, 44.77; H, 4.12; N, 23.11; V, 14.19%. IR (ATR) [cm^{-1}]: 3618(vw), 3113(vw), 2475(vw), 1548(s), 1504(w), 1436(m), 1405(s), 1307(s), 1209(s), 1115(m), 1045(s), 966(vs), 940(m), 755(s), 714(vs), 658(m), 620(m), 554(m), 450(w).

2.2. Measurements

Elemental analyses for C, H, and N were obtained at the Service Center of the Elementary Analysis of Organic Compounds, Faculty of Science, Kyushu University. Vanadium analyses were conducted using a titrimetric method [29]. Infrared spectra were recorded on a Bruker VERTEX70-S FT-IR Spectrometer using the ATR (Attenuated Total Reflection) method. Reflection spectra were recorded on an Ocean Optics USB2000+ Fiber Optic Spectrometer (Ocean Optics Inc., Dunedin, FL, USA). Magnetic susceptibilities were measured on a Quantum Design MPMS-XL5R SQUID susceptometer (Quantum Design, Inc., San Diego, CA, USA) under an applied magnetic field of 0.1 T in the temperature range 2–300 K. Diamagnetic corrections were applied using Pascal's constant [30].

2.3. Single Crystal X-Ray Diffraction

Diffraction data were measured on a Rigaku Vari-Max Saturn CCD 724 diffractometer (Rigaku Corp, Tokyo, Japan) with graphite monochromated Mo Ka radiation (λ = 0.71069 Å) at the Analytical Research Center for Experimental Sciences, Saga University. Data collections were carried on using CrystalClear SM 2.0 r16 [31]. The crystals were maintained at 293 K during data collection, and multi-scan correction for absorption was applied. Data processing was performed using CrysAlis Pro 42.49 [32]. Crystallographic data and experimental parameters are summarized in Table 1. Structures were solved using direct methods (ShelXT-2014/5) [33] and refined using ShelXL-2016/6 [34]. Non-hydrogen atoms were refined anisotropically, while hydrogen atoms were placed in calculated positions and refined using a riding model. μ-OH hydrogen atoms were identified from Fourier maps. Solvent masks were applied for disordered solvent molecules in **1** and **2** [35]. A total of 448 electrons and 400 electrons were found within a volume of 2370 $Å^3$ across two voids per unit cell for **1** and **2**, respectively, consistent with the presence of two C_2H_5OH molecules per molecular formula. Olex2-1.5 [36] was used as an interface to the ShelX program package. The structure drawings of the molecules were created using Mercury-2022.1.0 [37].

Table 1. Crystallographic data and refinement parameters.

	1	**2**	**3**	**4**	**5**
Empirical formula	$C_{21}H_{26}B_2N_{12}O_5V_2$, $2[C_2H_5OH]$	$C_{23}H_{30}B_2N_{12}O_5V_2$, $2[C_2H_5OH]$	$C_{24}H_{32}B_2N_{12}O_5V_2$	$C_{32}H_{32}B_2N_{12}O_5V_2$	$C_{38}H_{36}B_2N_{12}O_5V_2$
Formula weight	742.17	770.22	692.11	788.19	864.29
Temperature/K	293	293	293	293	293
Crystal system	monoclinic	monoclinic	monoclinic	orthorhombic	monoclinic
Space group	*C*2/*c*	*C*2/*c*	$P2_1/c$	$Pna2_1$	$P2_1/c$
a/Å	34.3359(8)	34.6189(3)	14.2258(6)	26.3453(6)	9.2537(4)
b/Å	14.6118(8)	14.8785(4)	14.9857(5)	11.5681)2)	31.5883(10)
c/Å	15.4430(10)	15.5866(4)	16.1012(7)	12.1916(3)	14.0235(6)
α/°	90	90	90	90	90
β/°	101.540(2)	99.784(2)	107.783(5)	90	96.528(4)
γ/°	90	90	90	90	90
V/Å^3	7591.3(3)	7911.5(4)	3268.5(2)	3715.57(14)	4072.6(3)
Z	8	8	4	4	4
D_{calc}/g cm^{-3}	1.299	1.293	1.406	1.409	1.410
μ/mm^{-1}	0.547	0.527	0.625	0.560	0.518
F (0 0 0)	3072.0	3200.0	1424.0	1616.0	1776.0
Crystal dimensions/mm^3	0.31 × 0.13 × 0.12	0.47 × 0.20 × 0.10	0.23 × 0.15 × 0.15	0.37 × 0.14 × 0.14	0.16 × 0.07 × 0.06
Radiation	MoKα	MoKα	MoKα	MoKα	MoKα
2*θ* range/°	3.038 to 61.808	2.986 to 61.764	3.006 to 62.046	3.846 to 61.994	3.194 to 61.948
Reflections collected	33,550	33,813	27,691	32,161	35,133
Independent reflections	10,842	10,408	8843	10,471	11,395
Data/Restraints/Params	10,842/2/383	18,867/126/1014	8843/11/461	10,471/1/481	11,395/1/535
Goodness of fit indicator	0.990	1.056	1.008	1.017	0.979
R indices [*I* > 2.00 s (*I*)]	R_1 = 0.0555 wR_2 = 0.13858	R_1 = 0.0469 wR_2 = 0.1222	R_1 = 0.0729 wR_2 = 0.1676	R_1 = 0.0423 wR_2 = 0.0857	R_1 = 0.0697 wR_2 = 0.1138
R indices (all data)	R_1 = 0.0923 wR_2 = 0.1554	R_1 = 0.0723 wR_2 = 0.1319	R_1 = 0.1423 wR_2 = 0.2038	R_1 = 0.0622 wR_2 = 0.0927	R_1 = 0.1855 wR_2 = 0.1483
Largest peak, hole/e Å^{-3}	0.61, −0.26	0.43, −0.26	0.70, −0.50	0.31, −0.17	0.31, −0.39
Flack parameter	-----	-----	-----	−0.012(7)	-----
CCDC deposition number	2405794	2405795	2405796	2405797	2405798

2.4. Computational Study

Frontier molecular orbitals calculations of **1**–**6** were performed using density functional theory (DFT) using the Gaussian 16 Rev. A.03 program package [38]. The B3LYP hybrid exchange–correlation functional with the 6-31G(d,p) basis set was used for all calculations. The calculation results were visualized using GaussView 6.1.1 [39].

3. Results and Discussion

3.1. Structural Studies

Single-crystal X-ray structural analysis (SC-XRD) confirmed that complexes **1**–**5** are μ-hydroxo-μ-carboxylato hetero-bridged dinuclear oxidovanadium(IV) complexes, with $\{HB(pz)_3\}^-$ serving as terminal ligands. These complexes are represented by the general formula $[(VO)_2\{HB(pz)_3\}_2(OH)(O_2CR)]$. Their molecular structures are depicted in Figure 2, and packing diagrams are provided in Figures S1–S5. Atom numbering has been standardized for all complexes. Selected bond distances and angles for **1**–**5** are summarized in Tables 2 and 3. SC-XRD measurements were also attempted for **6** using the obtained single crystals, but sufficient reflection data could not be obtained, and thus the structure could not be determined.

The bond distances and bond angles around V(IV) ions are consistent across all complexes, exhibiting no significant variations. The geometry around the vanadium ions (V1 and V2) is octahedral, with the axial axis aligned along the V=O direction. The V=O bond distances range from 1.581(2) to 1.596(2) Å, consistent with the typical V=O double bond length. The arrangements of the V=O groups in dinuclear oxidovanadium complexes can be classified based on their orientation relative to the V_2O_2 plane (*orthogonal, coplanar, twist*) and the alignment of the two V=O groups (*syn*, *anti*) [26]. Complexes **1**–**5** are classified as *anti-orthogonal*. The V–N bond distances for the pyrazolyl nitrogen atoms trans to the oxide ions (V1–N1 and V2–N7) are 2.2862(15)–2.322(3) Å, approximately 0.2 Å longer than other V–N distances (2.091(3)–2.1347(15) Å). This elongation is attributed to the strong trans-influence of the oxide ions. The equatorial coordination sites are occupied by the bridging hydroxo oxygen atom (O3), the bridging carboxylato oxygen atoms (O4 for V1 and O5 for V2), and two nitrogen atoms in pyrazolyl rings (N3 and N5 for V1, and N9 and

N11 for V2). The vanadium ions are not located within the equatorial plane but are elevated by approximately 0.26 Å toward the oxo ion. In complexes **1–4**, the difference in elevation between V1 and V2 is less than 0.01 Å, making them nearly identical. However, in Complex **5**, V1 is elevated by 0.2601 Å and V2 by 0.2794 Å, showing a slight difference. The bridging O3 atoms are presumed to be hydroxo ions (OH^-) rather than oxide ions (O^{2-}), as the V1–O3 and V2–O3 bond distances (1.9750(15)–2.000(2) Å) are more than 0.1 Å longer than the typical V–O distance (~1.85 Å) in mixed-valence μ-oxo bridged dioxidovanadium(IV, V) complexes [40,41]. These findings confirm that these complexes are hydroxo-bridged dinuclear oxidovanadium(IV) complexes. The tridentate $\{HB(pz)_3\}^-$ ligands show minimal distortion and effectively stabilize the dinuclear structures as terminal ligands. In complexes **1–3**, which are bridged by aliphatic carboxylates, the terminal carbon atoms of the alkyl chains show significant displacement. Notably, in Complex **3**, the t-butyl group is disordered in a 0.52:0.48 ratio.

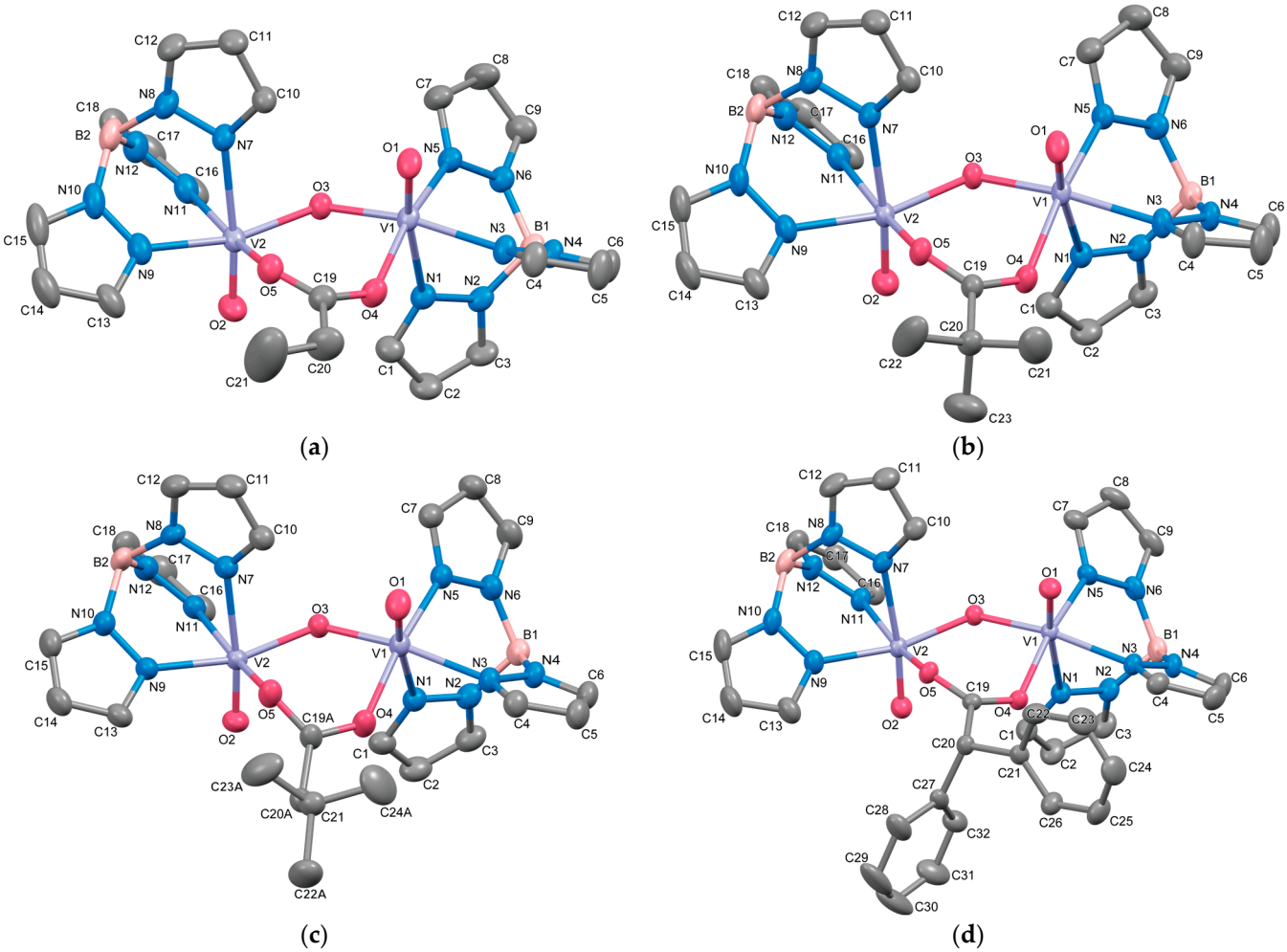


Figure 2. *Cont.*

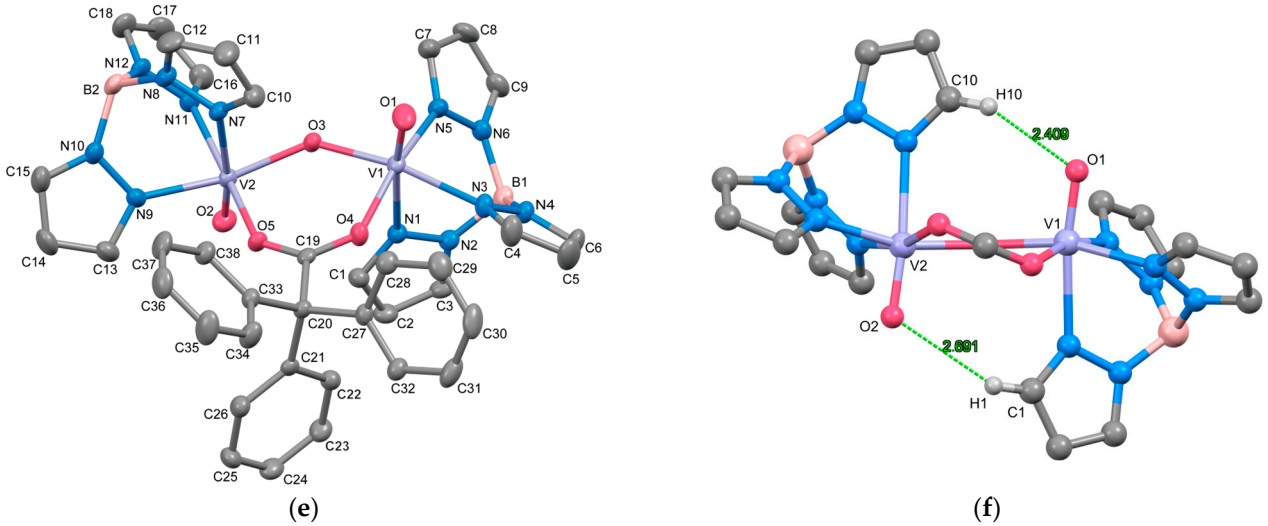


Figure 2. Crystal structures of **1**–**5**, shown with thermal ellipsoids at the 25% probability level. Hydrogen atoms are omitted for clarity. (**a**) Complex **1**. (**b**) Complex **2**. (**c**) Complex **3**, showing only the disordered 3,3-dimethylbutanoate unit with larger occupancy. (**d**) Complex **4**. (**e**) Complex **5**. (**f**) Intramolecular interactions in **1** (green dotted lines) between oxide ions and hydrogen atoms of the $\{HB(pz)_3\}^-$ ligands.

Table 2. Selected bond distances (Å) of **1**–**5**.

Bond	1	2	3	4	5
V1–O1	1.5943(15)	1.5901(13)	1.583(3)	1.596(2)	1.581(2)
V1–O3	1.9903(15)	1.9883(13)	1.983(2)	1.988(2)	2.000(2)
V1–O4	2.0175(16)	2.0338(14)	2.017(3)	2.036(2)	2.021(2)
V1–N1	2.2962(17)	2.2862(15)	2.287(3)	2.294(3)	2.305(3)
V1–N3	2.1180(17)	2.1347(15)	2.118(3)	2.121(3)	2.114(3)
V1–N5	2.0918(18)	2.0973(16)	2.091(3)	2.115(2)	2.096(3)
V2–O2	1.5921(16)	1.5950(14)	1.585(3)	1.587(3)	1.585(2)
V2–O3	1.9750(15)	1.9754(13)	1.974(2)	1.983(2)	1.988(3)
V2–O5	2.0189(17)	2.0222(13)	2.011(3)	2.018(2)	2.016(2)
V2–N7	2.3143(18)	2.3153(16)	2.296(3)	2.313(3)	2.322(3)
V2–N9	2.1115(19)	2.1114(16)	2.119(3)	2.114(3)	2.126(3)
V2–N11	2.105(2)	2.1031(16)	2.101(3)	2.112(3)	2.110(3)
V1···V2	3.6119(5)	3.5972(5)	3.5780(8)	3.5938(7)	3.7009(9)

Table 3. Selected bond angles (°) of **1**–**5**.

Angle	1	2	3	4	5
O1–V1–O3	102.25(7)	102.03(6)	102.13(12)	100.95(12)	101.59(11)
O1–V1–O4	98.44(8)	97.89(7)	98.58(14)	96.46(11)	96.71(12)
O1–V1–N1	171.54(7)	172.73(6)	172.88(13)	173.35(12)	173.26(12)
O3–V1–N3	163.97(7)	162.80(6)	162.24(11)	163.31(11)	163.29(10)
O4–V1–N5	165.68(7)	167.68(6)	166.37(12)	167.58(11)	167.21(11)
N3–V1–N5	85.93(7)	85.42(6)	86.36(11)	87.28(11)	86.17(11)
O2–V2–O3	101.19(8)	102.01(7)	101.77(12)	101.13(12)	103.18(12)
O2–V2–O5	98.54(9)	98.30(7)	98.84(13)	98.15(12)	99.05(10)
O2–V2–N7	173.30(8)	173.34(7)	172.67(14)	173.52(12)	171.80(11)
O3–V2–N9	164.14(8)	163.20(6)	161.73(11)	166.12(12)	161.94(10)
O5–V2–N11	165.22(7)	166.08(6)	166.67(12)	163.29(11)	166.21(10)
N9–V2–N11	84.73(8)	84.99(6)	85.52(12)	85.81(12)	86.26(11)
V1–O3–V2	131.26(8)	130.33(7)	129.48(12)	129.64(11)	136.25(12)

The torsion angles (α and β) related to the coordinating carboxylato oxygen atoms and the twist angles (ω) for the V1···V2 and O4···O5 lines are summarized in Table 4 (definitions shown in Figure 3). The carboxylato bridging modes are classified based on these parameters [42]. For complexes **1–4**, the absolute values of the α and β angles range from 140° to 156°, and the ω angles are approximately 30°, classifying these complexes as (*skew–skew, non-planar*) types. In contrast, for Complex **5**, the α and β angles are 173.61(13)° and −175.14(13)°, respectively, with an ω angle of 0.60(8)°, indicative of a (*syn–syn*, *coplanar*) type. The *syn–syn* bridging observed in **5** is considered to result from steric repulsion caused by the bulky triphenyl group. In relation to the differences in bridging modes, the larger V1···V2 distance and V1–O3–V2 angle in **5** compared to **1–4**, as well as the difference in the elevation of V1 and V2 from the equatorial plane, expected that the magnetic properties of **5** may differ from those of the other complexes.

Table 4. Structural parameters and bridging modes of carboxylato bridges in **1–5**.

Complex	α/° V1–O4–C19–C20	β/° V2–O5–C19–C20	ω/° V1···V2/O4···O5	Bridging Mode
1	152.7(2)	−149.3(2)	24.38(6)	*skew–skew, non-planar*
2	152.20(13)	−142.16(15)	29.00(5)	*skew–skew, non-planar*
3	145.55(6) *	−150.1(6) *	31.36(11)	*skew–skew, non-planar*
4	155.4(19)	−141.86(19)	27.74(9)	*skew–skew, non-planar*
5	173.61(13)	−175.14(13)	0.60(8)	*syn–syn, coplanar*

* Average value of disorder parts.

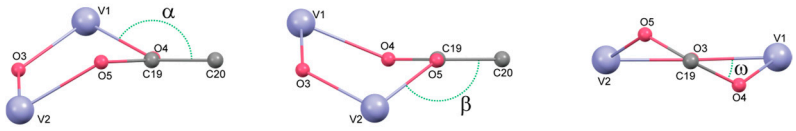


Figure 3. Definitions of the torsion angles (α and β) and twist angle (ω).

Intramolecular interactions are observed between the O1 and O2 atoms and the hydrogen atoms of the $\{HB(pz)_3\}^-$ ligands. Figure 2f illustrates the intramolecular short contacts, O1···H10–C10 and O2···H1–C1, in **1**, while the contact distances and angles for **1–5** are summarized in Table 5. The O1 and O2 atoms are each in close proximity to the hydrogen atoms at the 3 position of the pyrazolato rings located trans to one another, which are believed to contribute to the stabilization of the dinuclear structure. Since none of the complexes possess a centrosymmetric structure, differences of 0.2–0.3 Å in O···H distances and 5–10° in O···H–C angles are observed between V1 and V2.

Table 5. Intramolecular short contacts for O1 and O2.

Complex	O1···H10/Å	O1···H10–C10/°	O2···H1/Å	O2···H1–C1/°
1	2.4093(15)	152.54(13)	2.6905(17)	142.09(15)
2	2.4307(14)	150.84(12)	2.7057(14)	143.92(13)
3	2.471(3)	150.4(2)	2.660(3)	147.1(2)
4	2.638(3)	149.3(2)	2.430(3)	145.9(3)
5	2.675(2)	139.1(2)	2.481(2)	132.4(2)

Additionally, intermolecular interactions are observed between the O1 and O2 atoms and the hydrogen atoms of the $\{HB(pz)_3\}^-$ ligands in neighboring molecules. Hirshfeld surface analysis was performed for **1–5** using CrystalExplorer 3.1 [43]. The resulting Hirshfeld surface (d_{norm}) for **1** is shown in Figure 4a. The surface is mapped in red near the vanadyl oxygen atoms and the hydrogen atoms of the pyrazolato rings, highlighting the presence of strong interactions. The 2D fingerprint plots for O···H interactions are presented in Figure 4b (for **1**) and Figure S6 (for **2–5**). The fingerprint plots reveal two

characteristic sharp spikes, indicating specific contacts between complex molecules, as seen in Figure 4a.

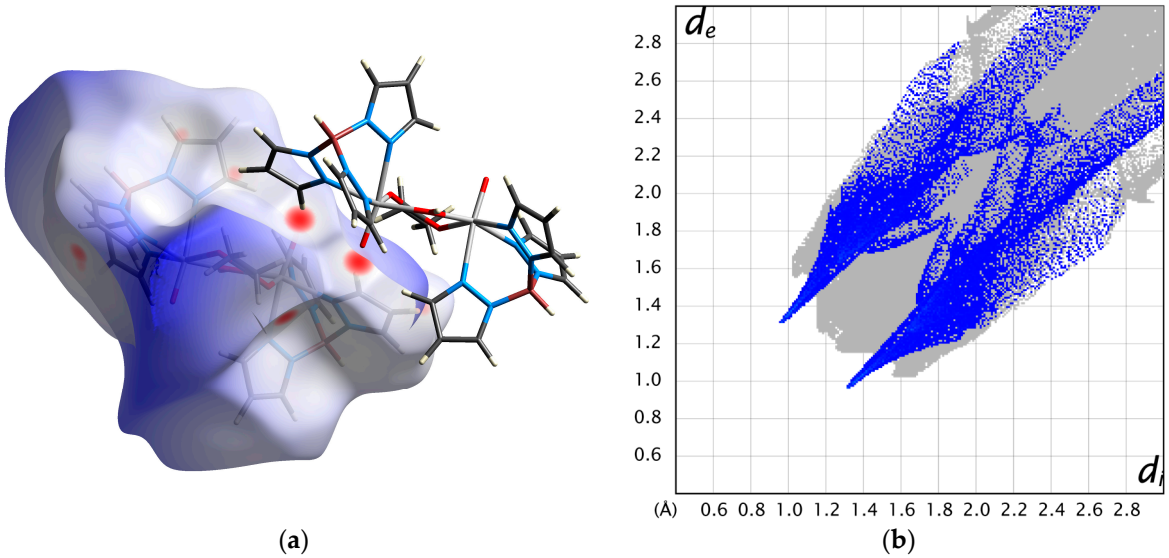


Figure 4. (**a**) Hirshfeld surface (d_{norm}) for **1**. (**b**) 2D fingerprint plot for O···H contacts.

3.2. IR Spectra

The FT-IR spectra of complexes **1**–**6** are shown in Figure S7, and the characteristic bands are summarized in Table 6. The ν(OH) stretching vibrations of the bridging hydroxo group were observed at 3618–3634 cm^{-1}, while the ν(BH) stretching vibration of the hydroborate ion appeared at 2465–2485 cm^{-1} [44]. These results corroborate the single-crystal X-ray analysis, confirming that the bridging O3 is a μ-hydroxo ion rather than a μ-oxo ion and that the terminal ligands are coordinated as hydrotris(pyrazolyl)borates. The asymmetric and symmetric carboxylate stretching bands, ν_{as}(COO) and ν_s(COO), were observed at 1517–1586 cm^{-1} and 1404–1406 cm^{-1}, respectively. The separation values (Δ) between ν_{as}(COO) and ν_s(COO) for all complexes, except for **5**, fall within a similar range (111–154 cm^{-1}). In contrast, Complex **5** exhibits a larger Δ value of 182 cm^{-1}, consistent with its *syn–syn* bridging mode, which differs from the bridging modes observed in the other complexes [45]. The ν(V=O) stretching vibrations were observed at 966–970 cm^{-1}, comparable to those typically observed in vanadyl (V=O) complexes [46,47]. Based on these IR data, the bridging structure of **6**, which was not structurally analyzed by single-crystal X-ray diffraction, is predicted to adopt a *skew–skew* non-planar type, similar to that of **4**.

Table 6. Relevant FT-IR data (cm^{-1}) for **1–6**.

Complex	ν(OH)	ν(BH)	ν_{as}(COO)	ν_s(COO)	Δ(ν_{as} − ν_{as})	ν(V=O)
1	3622	2485	1541	1405	136	967
2	3626	2471	1517	1406	111	969
3	3627	2472	1522	1405	117	970
4	3643	2476	1558	1404	154	967
5	3633	2465	1586	1404	182	968
6	3618	2475	1548	1405	143	966

3.3. Electronic Spectra

The electronic spectra of the present complexes were recorded using the diffuse reflectance technique. The spectra are shown in Figure 5, and the corresponding wavenumbers of the absorption bands are listed in Table 7. For all complexes, two absorption peaks and a shoulder attributed to *d-d* transitions were observed at approximately 13.6 × 10^3, 18.0 × 10^3, and around 30 × 10^3 cm^{-1}. These transitions are assigned to the $^2B_2 \rightarrow {}^2E$,

$^2B_2 \rightarrow {}^2B_1$, and $^2B_2 \rightarrow {}^2A_1$ transitions, respectively, originating from the tetragonally distorted oxidovanadium(IV) center [48]. Additionally, shoulder bands around 38×10^3 cm^{-1} were observed, which are attributed to metal-to-ligand charge transfer (MLCT) transitions involving the $\{HB(pz)_3\}^-$ ligands [19]. The shoulder observed around 33×10^3 cm^{-1} in **5** is thought to result from the slight differences in the geometries of the two vanadium centers in this complex, as mentioned in Section 3.1. This geometric difference may cause the broad CT band originating from the $\{HB(pz)_3\}^-$ ligands to split, making it distinguishable in **5**.

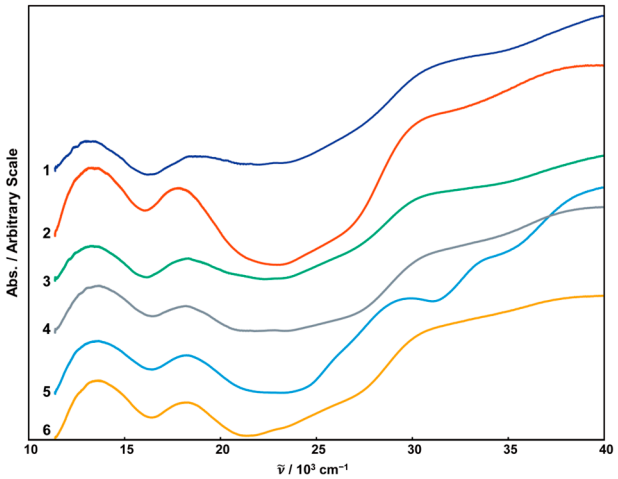


Figure 5. Diffuse reflectance spectra of powder samples for **1–6.**

Table 7. Spectral data for d-d transitions ($\tilde{\nu}/10^3$ cm^{-1}) of **1–6.**

Complex	$^2B_2 \rightarrow {}^2E$	$^2B_2 \rightarrow {}^2B_1$	$^2B_2 \rightarrow {}^2A_1$
1	13.1	18.4	30.3 ^{sh}
2	13.3	17.8	29.6 ^{sh}
3	13.3	18.3	30.0 ^{sh}
4	13.7	18.2	30.2 ^{sh}
5	13.7	18.2	29.9
6	13.6	18.3	30.0 ^{sh}

^{sh} Shoulder.

3.4. Magnetic Properties

Magnetic susceptibility measurements were performed using a SQUID (superconducting quantum interference device) magnetometer. The temperature dependence of the $\chi_M T$ values for **1** is shown in Figure 6, while data for the other complexes are presented in Figure S8. At 300 K, the $\chi_M T$ value for **1** is 0.785 cm^3 mol^{-1} K, which is slightly higher than the spin-only value of 0.75 cm^3 mol^{-1} K expected for two uncoupled V(IV) ions ($S = 1/2$). The $\chi_M T$ values remain nearly constant down to 100 K, gradually increase to a peak at 20 K, and then decrease slightly at a lower temperature. The $1/\chi_M$ plots are nearly linear, and the Curie-Weiss constant (θ), calculated from the least-squares fit, is positive (+2.727 K), indicating weak ferromagnetic interaction between the V(IV) ions in **1**. The decrease in the $\chi_M T$ value below 20 K is likely due to zero-field splitting or intermolecular interactions. The magnetic behavior of the other complexes closely resembles that of **1** (Figure S8).

These magnetic behaviors were analyzed using Equation (1) [49], which incorporates intermolecular interactions (zJ') into the Bleaney–Bowers Equation (2).

$$\chi_{corr} = \frac{\chi}{1 - \left(\frac{zJ'}{N\mu^2}\right)\chi} \quad (1)$$

$$\chi = \frac{Ng^2\beta^2}{kT}\frac{1}{3 + e^{-\frac{2J}{kT}}} + \text{TIP} \quad (2)$$

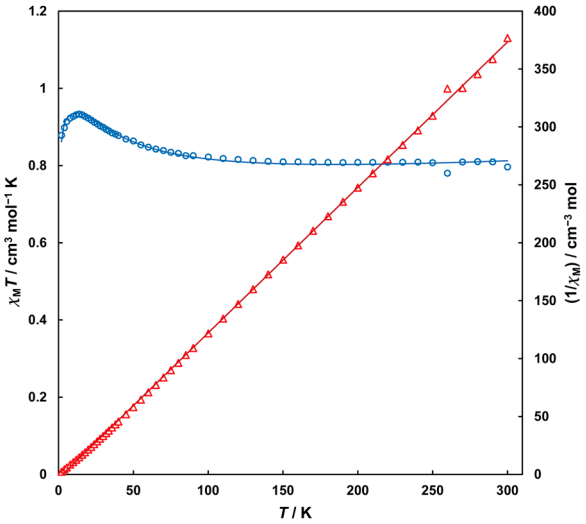


Figure 6. Temperature dependence of $\chi_M T$ (blue circles) and $1/\chi_M$ (red triangles) vs. T plots for **1**. Solid lines represent best-fitted parameters as described in the text.

The best-fit parameters were determined using a Simplex non-linear least squares calculation using the PHI ver. 3.1.6 program [50]. The resulting magnetic parameters are summarized in Table 8. The analysis revealed ferromagnetic interactions of approximately 20 cm^{-1} between the V(IV) ions in all complexes. The *anti-orthogonal* type in the classification of dinuclear oxidovanadium(IV) complexes by Plas et al. [26] is thought to exhibit strong antiferromagnetic interactions due to direct interactions between d_{xy} orbitals. Therefore, it is particularly intriguing that the present complexes, despite being classified as *anti-orthogonal*, were confirmed to exhibit pronounced ferromagnetic interactions.

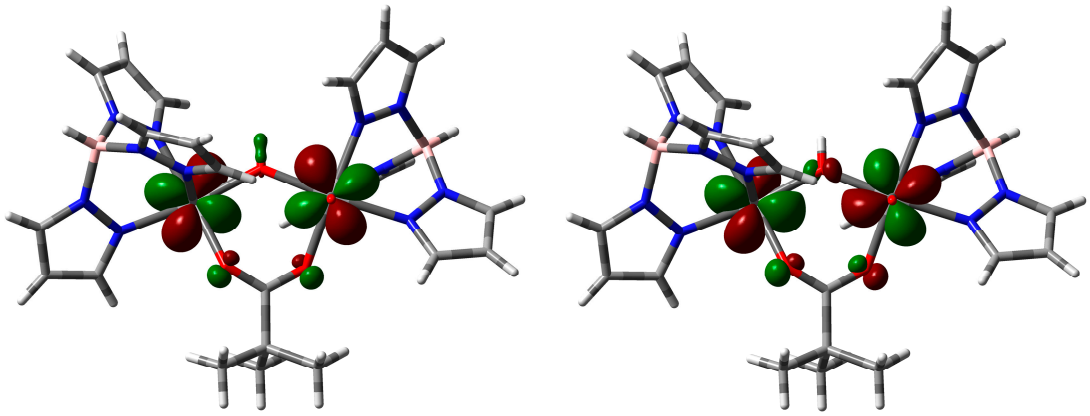
Table 8. Magnetic parameters for **1–6.**

Complex	J/cm^{-1}	g	TIP /10^{-6} cm^3 mol^{-1}	zJ/cm^{-1}	$\chi_M T$ (300 K) /cm^3 mol^{-1} K	θ/K
1	19.51	1.944	174	−0.041	0.785	2.727
2	19.33	1.917	398	−0.050	0.842	0.575
3	23.26	1.978	381	−0.043	0.889	1.336
4	19.20	1.966	210	−0.036	0.803	2.892
5	17.04	1.916	257	−0.026	0.782	2.927
6	20.90	1.982	382	−0.021	0.887	1.246

The singly occupied molecular orbitals (SOMOs) obtained from the Gaussian 16 calculations are illustrated in Figure 7. In the present complexes, the V···V distances are sufficiently large due to the presence of the μ-carboxylato bridge, preventing direct interactions. Furthermore, no superexchange pathways are observed in the asymmetric SOMO (ψ_{as}, Figure 7a). While a potential exchange pathway exists via the μ-hydroxo bridge in the symmetric SOMO (ψ_s, Figure 7b), the exchange interaction is considered weak. These quantum chemical calculations are consistent with the magnetic analysis results, indicating that complexes **1**−**6** exhibit ferromagnetic interactions ($J \sim 20$ cm^{-1}) despite being classified as *anti-orthogonal* types.

Magneto-structural correlations have been extensively studied for homo-bridged complexes, such as those with monoatomic or diatomic double bridges [18,24]. However, hetero-bridged complexes, like those investigated in this study, remain largely unexplored. Here, the dinuclear oxidovanadium(IV) complexes were categorized into three groups based on the type of bridging: (A) monoatomic bridges, (B) diatomic bridges, and (C) hetero bridges. The relevant structural parameters and J values of **1–6**, along with the

data from related complexes, are summarized in Table 9 for each group. While no strong correlations were observed between the *J* values and V···V distances or V–O–V angles, a moderate correlation with the dihedral angle (τ) formed by the two vanadium planes was found across all three groups, as shown in Figure 8. In Groups A and B, the *J* values were highly dependent on changes in τ, and interestingly, opposite correlation trends were observed between the two groups. For Group C, while the deviations in both *J* and τ values are small, making definitive conclusions difficult, there appears to be a potential correlation where smaller dihedral angles (τ), approaching a planar configuration, are associated with smaller *J* values. This phenomenon is thought to arise from improved planarity of the dinuclear plane, which enhances the contribution of the superexchange pathway through the hydroxo-bridged site. The amplification of this superexchange pathway is thought to enhance the antiferromagnetic interaction, resulting in smaller *J* values. The present complexes **1–6** share the same terminal ligands and hydroxo bridges, resulting in similar geometries around the vanadium ions. This is thought to contribute to the relatively small differences in *J* values. To further the investigation, it is necessary to increase the number of examples of complexes combining various terminal ligands, monoatomic bridges, and carboxylato bridges and elucidate their structures and magnetic properties.



(**a**) (**b**)

Figure 7. SOMOs of **2**, computed using the Gaussian 16 software package. (**a**) Asymmetric SOMO (ψ_{as}). (**b**) Symmetric SOMO (ψ_{s}).

Table 9. Experimental exchange coupling constants *J* for double-bridged dinuclear oxidovanadium(IV) complexes and characteristic structural parameters. **a–l** represent assignment symbols for the referenced complexes, while **1–6** denote the present complexes. t.w. = This work.

Complex [a]		*J* /cm^{-1}	τ /°	V···V /Å	V–O–V /°	V=O Configuration	Ref.
A: *monoatomic bridge*							
$[(VO)_2(tacn)(OH)]_2Br_2$	**a**	−177	0	3.033	101.2	*anti*	[10]
$[(VO)(L^1)]_2^{2+}$	**b**	−167.9	0	3.125	98.6	*anti*	[11]
$[(VO)_2(OH)_2(tpen)]I_2$	**c**	−150	4.3	2.965	98.0 [av]	*syn*	[12]
$[(VO)_2(cit)(Hcit)]^{3-}$	**d**	−212	7.4	2.949	97.8 [av]	*syn*	[13]
$[(VO)_2(L^2)(SO_4)]$	**e**	−128	29.9	3.077	99.4	*syn*	[14]
$[(VO)_2(L^2)(OCH_3)(DMSO)]$	**f**	−122	48.9	3.026	98.1 [av]	*anti*	[15]
$[(VO)(L^3)]_2^{2+}$	**g**	9	69	3.122	96.3 [av]	*syn*	[16]
B: *diatomic bridge*							
$[(VO)(L^4)(SO_4)(CH_3OH)]_2$	**H**	−14.8	0	4.631	—	*anti*	[17]
$[(VO)\{HB(pz)_3\}(O_2PPh_2)]_2$	**I**	−11.75	0	5.27	—	*anti*	[18]
$[(VO)\{HB(pz)_3\}(O_2PHPh)_2]_2$	**J**	−40.65	11.2	5.136	—	*anti*	[18]
$[(VO)(tmtacn)(O_2CCH_3)]_2I_2$	**k**	−114	67.1	4.075	—	*syn*	[19]

Table 9. *Cont.*

Complex [a]		J /cm^{-1}	τ /°	V···V /Å	V–O–V /°	V=O Configuration	Ref.
C: *hetero bridge*							
$[(VO)_2\{HB(pz)_3\}_2(OH)(O_2CH_2CH_3)]$	**1**	19.51	17.4	3.612	130.9	*anti*	t.w.
$[(VO)_2\{HB(pz)_3\}_2(OH)(O_2C$-*t*-Bu$)]$	**2**	19.33	23.3	3.597	130.3	*anti*	t.w.
$[(VO)_2\{HB(pz)_3\}_2(OH)(O_2CCH_2$-*t*-Bu$)]$	**3**	23.26	26.0	3.578	129.7	*anti*	t.w.
$[(VO)_2\{HB(pz)_3\}_2(OH)(O_2CHPh_2)]$	**4**	19.20	20.0	3.594	129.4	*anti*	t.w.
$[(VO)_2\{HB(pz)_3\}_2(OH)(O_2CPh_3)]$	**5**	17.04	5.0	3.701	136.2	*anti*	t.w.
$[(VO)_2\{HB(pz)_3\}_2(OH)(O_2CCH_2CH_2Ph)]$	**6**	20.90	—-	—-	—-	—-	t.w.
$[(VO)_2\{HB(pz)_3\}_2(OH)(O_2CCH_3)]$	**l**	>0 [b]	14.8	3.621	131.6	*anti*	[18]

[a] Ligand abbreviations: tacn = 1,4,7-triazacyclononane, H_2L^1 = *N*,*N*-bis(2-hydroxybenzyl)aminoacetic acid, tpen = *N*,*N*,*N*′,*N*′-tetrakis(2-pyridylmethyl)ethylenediamine, H_4cit = citric acid, HL^2 = 2,6-bis(salicylideneaminomethyl)-4-methylphenol, HL^3 = bis(benzenethiolato)methylsilanoxide, L^4 = bis(benzenethiolato)phenylphosphine oxide. [b] The *J* value has not been specifically analyzed. *av* Average angles.

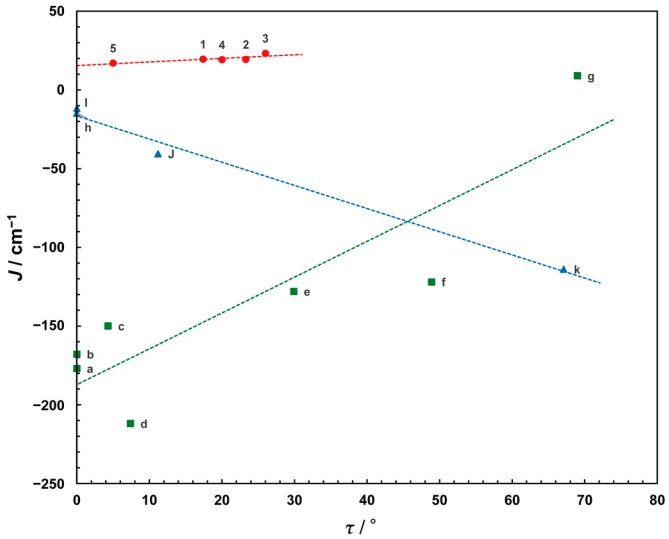


Figure 8. Magneto-structural correlations between the dihedral angles (τ) of the equatorial planes and the *J* values. Green squares represent Group A (monoatomic bridges), blue triangles represent Group B (diatomic brides), and red circles represent Group C (hetero bridges). Dotted lines in each color indicate the least squares fit for each group.

4. Conclusions

New dinuclear oxidovanadium(IV) complexes **1**−**6** were synthesized. The crystal structures were elucidated using single-crystal X-ray analysis, revealing that all complexes adopt a μ-hydroxo-μ-carboxylato hetero-bridged dinuclear structure with $\{HB(pz)_3\}^-$ as terminal ligands. The arrangement of the two V=O groups was classified as *anti-orthogonal*. Magnetic measurements revealed the presence of ferromagnetic interactions between the V(IV) ions. Interestingly, the observed *J* values deviate from the range predicted by the magneto-structural correlations typically associated with *anti-orthogonal* configurations in dinuclear oxidovanadium(IV) complexes. These results suggest that the hetero-bridged structure plays a critical role in facilitating ferromagnetic interactions in the dinuclear oxidovanadium(IV) complexes.

Supplementary Materials: The following supporting information can be downloaded at https://www.mdpi.com/article/10.3390/cryst14121072/s1, Figure S1. Crystal packing diagrams of **1**. Figure S2. Crystal packing diagrams of **2**. Figure S3. Crystal packing diagrams of **3**. Figure S4. Crystal packing diagrams of **4**. Figure S5. Crystal packing diagrams of **5**. Figure S6. 2D fingerprint plot for O···H contacts of **2**–**5**. Figure S7. IR spectra of complexes **1**–**6**. Figure S8. Temperature dependence of $\chi_M T$(blue circles) and $1/\chi_M$ (red triangles) vs. T plots of **2**–**6**. Solid lines are drawn with the best-fitted parameter values described in the text.

Author Contributions: Conceptualization, T.T.; Data Curation, M.K. and T.T.; Formal Analysis, R.Y. and M.K.; Funding Acquisition, M.K.; Investigation, R.Y.; Project Administration, M.K. and T.T.; Software, M.K.; Supervision, M.K. and T.T.; Visualization, M.K.; Writing—Original Draft, M.K.; Writing—Review and Editing, M.K. All authors have read and agreed to the published version of the manuscript.

Funding: This research received no external funding.

Data Availability Statement: The data that support the findings of this study are available from the author upon reasonable request.

Acknowledgments: This research was performed using the equipment (IR and single-crystal X-ray analysis) of the Analytical Research Center for Experimental Science, Saga University. The authors thank the Service Center of the Elementary Analysis of Organic Compounds, Faculty of Science, Kyushu University for elementary analysis.

Conflicts of Interest: The authors declare no conflicts of interest. The funders had no role in the design of this study; in the collection, analyses, or interpretation of data; in the writing of the manuscript; or in the decision to publish the results.

References

1. Sultana, S.Y.; Sharma, M.; Talukdar, H.; Begum, T.; Gour, N.K.; Sharma, B.; Islam, N.S. New mixed ligand oxido-vanadium(V) complexes with O,O-donor and diimine ligands: Synthesis, crystal structure and catalytic activity in eco-friendly oxidation of olefins and phenol. *Mol. Catal.* **2024**, *565*, 114352. [CrossRef]
2. Sutradhar, M.; Martins, L.M.D.R.S.; da Silva, M.F.C.G.; Pombeiro, A.J.L. Vanadium complexes: Recent progress in oxidation catalysis. *Coord. Chem. Rev.* **2015**, *301*, 200–239. [CrossRef]
3. Kumar, A.; Sasai, H.; Takizawa, S. Atroposelective synthesis of C–C axially chiral compounds via mono- and dinuclear vanadium catalysis. *Acc. Chem. Res.* **2022**, *55*, 2949–2965. [CrossRef] [PubMed]
4. Zhang, H.; Zhang, M.; Jia, Y.; Geng, L.; Yin, B.; Li, S.; Luo, Z.; Pan, F. Vanadium cluster neutrals reacting with water: Superatomic features and hydrogen evolution in a fishing mode. *J. Phys. Chem. Lett.* **2021**, *12*, 1593–1600. [CrossRef] [PubMed]
5. Yang, Y.; Fu, Y.; Tian, Y.; Zhao, L.; Qin, C.; Wang, X.; Su, Z. Efficient iodine capture by metal–organic cubes based on hexanuclear vanadium clusters. *Inorg. Chem. Front.* **2023**, *10*, 6221–6228. [CrossRef]
6. Aureliano, M.; Gumerova, N.I.; Sciortino, G.; Garribba, E.; McLauchlan, C.C.; Rompel, A.; Crans, D.C. Polyoxidovanadates' interactions with proteins: An overview. *Coord. Chem. Rev.* **2022**, *454*, 214344. [CrossRef]
7. Baran, E.J. Structural and spectroscopic studies related to vanadium chemistry and biochemistry. *Coord. Chem. Rev.* **2024**, *502*, 215549. [CrossRef]
8. Mubarak, M.Q.E.; Gérard, E.F.; Blanford, C.F.; Hay, S.; Visser, S.P. How do vanadium chloroperoxidases generate hypochlorite from hydrogen peroxide and chloride? A computational study. *ACS Catal.* **2020**, *10*, 14067–14079. [CrossRef]
9. Treviño, S.; Díaz, A.; Sánchez-Lara, E.; Sanchez-Gaytan, B.L.; Perez-Aguilar, J.M.; González-Vergara, E. Vanadium in biological action: Chemical, pharmacological aspects, and metabolic implications in diabetes mellitus. *Biol. Trace Elem. Res.* **2019**, *188*, 68–98. [CrossRef]
10. Wieghardt, K.; Bossek, U.; Volckmar, K.; Swiridoff, W.; Weiss, J. Synthesis and crystal structure of bis(μ-hydroxo)bis[oxo(1,4,7-triazacyclononane)vanadium(IV)] dibromide, a μ-hydroxo-bridged cation with antiferromagnetically coupled vanadium(IV) centers. *Inorg. Chem.* **1984**, *23*, 1387–1389. [CrossRef]
11. Ceccato, A.S.; Neves, A.; de Brito, M.A.; Drechsel, S.M.; Mangrich, A.S.; Werner, R.; Haase, W.; Bortoluzzi, A.J. Magneto-structural correlation for binuclear octahedral vanadium(IV)–oxo complexes. Synthesis, structure and magnetic properties of a $V^{IV}O^{2+}$ complex with a new ligand derived from glycine. *J. Chem. Soc. Dalton Trans.* **2000**, 1573–1577. [CrossRef]
12. Neves, A.; Wieghardt, K.; Number, B.; Weiss, J. Synthesis, magnetism and crystal structure of $[V_2O_2(\mu\text{-}OH)_2(tpen)]I_2{\cdot}4H_2O$; a binuclear complex containing the *syn*-$\{VO(\mu\text{-}OH)_2VO\}^{2+}$ core (tpen = tetrakis(2-pyridylmethyl)ethylenediamine). *Inorg. Chim. Acta* **1988**, *150*, 183–187. [CrossRef]
13. Burojevic, S.; Shweky, I.; Bino, A.; Summers, D.A.; Thompson, R.C. Synthesis, structure and magnetic properties of an asymmetric dinuclear oxocitratovanadate(IV) complex. *Inorg. Chim. Acta* **1996**, *251*, 75–79. [CrossRef]
14. Das, R.; Nanda, K.K.; Mukherjee, A.K.; Mukherjee, M.; Helliwell, M.; Nag, K. Macrocyclic oxovanadium(IV) complexes: Structure, magnetochemistry and electrochemistry. *J. Chem. Soc. Dalton Trans.* **1993**, 2241–2246. [CrossRef]
15. Mikuriya, M.; Fukuya, M. Synthesis, crystal structure, and magnetic property of a dinuclear oxovanadium(IV) complex with 2,6-bis(salicylideneaminomethyl)-4-methylphenol. *Bull. Chem. Soc. Jpn.* **1996**, *69*, 679–683. [CrossRef]
16. Tsai, Y.-F.; Huang, G.-S.; Yang, C.-I.; Tsai, H.-L.; Liu, Y.-H.; Kuo, T.-S.; Hsu, H.F. Dinuclear oxovanadium(IV) thiolate complexes with ferromagnetically coupled interaction between vanadium centers. *Inorg. Chem.* **2007**, *46*, 10467–10469. [CrossRef]
17. Bazhina, E.S.; Nikiforova, M.E.; Aleksandrov, G.G.; Efimov, N.N.; Ugolkova, N.A.; Nikitin, O.M.; Magdesieva, T.V.; Bogomyakov, A.S.; Minin, V.V.; Sidorov, A.A.; et al. New sulfate-bridged dinuclear oxidovanadium complexes. *Inorg. Chim. Acta* **2012**, *392*, 192–198. [CrossRef]

18. Dean, N.S.; Bond, M.R.; O'Connor, C.J.; Carrano, C.J. Structure and magnetism of dibridged vanadium(IV) hydrotris(pyrazolyl) borate dimers. *Inorg. Chem.* **1996**, *35*, 7643–7648. [CrossRef]
19. Koeppen, M.; Fresen, G.; Wieghardt, K.; Llusar, R.M.; Number, B.; Weiss, J. Syntheses and spectroscopic and magnetic properties of novel binuclear vanadium(III)/(IV) complexes. Crystal structures of $[L_2V_2(\mu\text{-}O)(\mu\text{-}CH_3CO_2)_2]I_2{\cdot}2H_2O$ and $[L_2V_2O_2(\mu\text{-}CH_3CO_2)_2]I_2$ (L = 1,4,7-trimethyl-1,4,7-triazacyclononane). *Inorg. Chem.* **1988**, *27*, 721–727. [CrossRef]
20. Roy, S.; Böhme, M.; Dash, S.P.; Mohanty, M.; Buchholz, A.; Plass, W.; Majumder, S.; Kulanthaivel, S.; Banerjee, I.; Reuter, H.; et al. Anionic dinuclear oxidovanadium(IV) complexes with azo functionalized tridentate ligands and μ-ethoxido bridge leading to an unsymmetric twisted arrangement: Synthesis, X-ray Structure, magnetic properties, and cytotoxicity. *Inorg. Chem.* **2018**, *57*, 5767–5781. [CrossRef]
21. Janas, Z.; Jezierska, J.; Ozarowski, A.; Bieńko, A.; Lis, T.; Jezierski, A.; Krawczyk, M. Investigation of vanadium(III) and vanadium(IV) compounds supported by the linear diaminebis(phenolate) ligands: Correlation between structures and magnetic properties. *Dalton Trans.* **2021**, *50*, 5184–5196. [CrossRef] [PubMed]
22. Lagostina, V.; Carniato, F.; Esteban-Gómez, D.; Platas-Iglesias, C.; Chiesa, M.; Botta, M. Magnetic and relaxation properties of vanadium(IV) complexes: An integrated 1H relaxometric, EPR and computational study. *Inorg. Chem. Front.* **2023**, *10*, 1999–2013. [CrossRef]
23. Roy, S.; Böhme, M.; Lima, S.; Mohanty, M.; Banerjee, A.; Buchholz, A.; Plass, W.; Rathnam, S.; Banerjee, I.; Kaminsky, W.; et al. Methoxido-bridged lacunary heterocubane oxidovanadium(IV) cluster with azo ligands: Synthesis, X-ray Structure, magnetic properties, and antiproliferative activity. *Eur. J. Inorg. Chem.* **2022**, *2022*, e202200109. [CrossRef]
24. Zhang, L.; Chen, Z. Magnetic exchange interaction in the μ-hydroxo bridged vanadium(IV) dimers: A density functional theory combined with broken-symmetry approach. *Chem. Phys. Lett.* **2001**, *345*, 353–360. [CrossRef]
25. Rodríguez-Fortea, A.; Alemany, P.; Alvarez, S.; Ruiz, E. A theoretical study of the exchange coupling in hydroxo- and alkoxo-bridged dinuclear oxovanadium(IV) compounds. *Eur. J. Inorg. Chem.* **2004**, *2004*, 143–153. [CrossRef]
26. Plass, W. Magneto-structural correlations in dinuclear d^1–d^1 complexes: Structure and magnetochemistry of two ferromagnetically coupled vanadium(IV) dimers. *Angew. Chem. Int. Ed. Engl.* **1996**, *35*, 627–731. [CrossRef]
27. Melero, M.M.; Kłosek, Z.; de Arellano, C.R.; Olmos, A. Synthesis of known and previously inaccessible poly(pyrazolyl)borates under mild conditions. *J. Org. Chem.* **2023**, *88*, 9130–9135. [CrossRef]
28. Kraft, S.J.; Fanwick, P.E.; Bart, S.C. Synthesis and characterization of a uranium(III) complex containing a redox-active 2,2′-bipyridine ligand. *Inorg. Chem.* **2010**, *49*, 1103–1110. [CrossRef]
29. Kaimal, V.R.M.; Shome, S.C. Direct titration of vanadium(IV) with EDTA using N-benzoyl-N-phenylhydroxylamine as metal indicator. *Anal. Chim. Acta* **1962**, *27*, 594–596. [CrossRef]
30. Selwood, P.W. *Magnetochemistry*; Interscience Publishers: New York, NY, USA, 1956; pp. 78–91.
31. Rigaku Corporation. *CrystalClear: Data Collection and Processing Software*; Rigaku Corporation: Tokyo, Japan, 1998.
32. Rigaku Oxford Diffraction. *CrysAlis Pro*; Rigaku Oxford Diffraction: Tokyo, Japan, 2022.
33. Sheldrick, G.M. SHELXT—Integrated space-group and crystal-structure determination. *Acta Crystallogr. Sect. A Found. Adv.* **2015**, *71*, 3–8. [CrossRef]
34. Sheldrick, G.M. Crystal structure refinement with SHELXL. *Acta Crystallogr. Sect. C Struct. Chem.* **2015**, *71*, 3–8. [CrossRef] [PubMed]
35. Jiang, J.-S.; Brünger, A.T. Protein hydration observed by X-ray diffraction: Solvation properties of penicillopepsin and neuraminidase crystal structures. *J. Molec. Biol.* **1994**, *243*, 100–115. [CrossRef] [PubMed]
36. Dolomanov, O.V.; Bourhis, L.J.; Gildea, R.J.; Howard, J.A.K.; Puschmann, H. OLEX2: A complete structure solution, refinement and analysis program. *J. Appl. Cryst.* **2009**, *42*, 339–341. [CrossRef]
37. Macrae, C.F.; Sovago, I.; Cottrell, S.J.; Galek, P.T.A.; McCabe, P.; Pidcock, E.; Platings, M.; Shields, G.P.; Stevens, J.S.; Towler, M.; et al. Mercury 4.0: From visualization to analysis, design and prediction. *J. Appl. Crystallogr.* **2020**, *53*, 226–235. [CrossRef] [PubMed]
38. Frisch, M.J.; Trucks, G.W.; Schlegel, H.B.; Scuseria, G.E.; Robb, M.A.; Cheeseman, J.R.; Scalmani, G.; Barone, V.; Petersson, G.A.; Nakatsuji, H.; et al. *Gaussian 16, Revision C.01*; Gaussian, Inc.: Wallingford, CT, USA, 2016.
39. Dennington, R.; Keith, T.A.; Millam, J.M. *GaussView, Version 6*; Semichem Inc.: Shawnee Mission, KS, USA, 2016.
40. Fukuda, I.; Matsushima, H.; Maeda, K.; Koikawa, M.; Tokii, T. The first example of μ-oxo-bis(μ-carboxylato)dioxovanadium(IV,V) complex. *Chem. Lett.* **1997**, *26*, 463–464. [CrossRef]
41. Richa; Kumar, A.; Verma, I.; Gautam, M.; Erande, R.D.; Kłak, J.; Choquesillo-Lazarte, D.; Mota, A.J.; Rajput, A.; Arora, H. Structural and magnetic characterization of mixed-valence vanadium (IV/V) complex with $\{(VO)_2(\mu\text{-}O)\}^{3+}$ core: Theoretical and experimental insights. *J. Mol. Struct.* **2022**, *1269*, 133805. [CrossRef]
42. Wei, P.-R.; Li, Q.; Leung, W.-P.; Makt, T.C.W. A dinuclear manganese(ll) complex doubly bridged by *skew-skew* μ-carboxylato groups: Synthesis and X-ray structure of $[\{Mn(bpy)_2(p\text{-}Me_2N^+C_5H_4NCH_2CO_2^-)\}_2](C1O_4)_4$. *Polyhedron* **1997**, *16*, 897–902. [CrossRef]
43. Spackman, M.A.; Jayatilaka, D. Hirshfeld surface analysis. *Cryst. Eng. Comm.* **2009**, *11*, 19–32. [CrossRef]
44. Ibrahim, M.M.; Mersal, G.A.M.; Fallatah, A.M.; Althubeiti, K.; El-Sheshtawy, H.S.; Taleb, M.F.A.; Das, M.R.; Boukherroub, R.; Attia, M.S.; Amin, M.A. Electrocatalytic hydrogen generation using tripod containing pyrazolylborate-based copper(II), nickel(II), and iron(III) complexes loaded on a glassy carbon electrode. *RSC Adv.* **2022**, *12*, 8030–8042. [CrossRef]

45. Deacon, G.B.; Phillips, R.J. Relationships between the carbon-oxygen stretching frequencies of carboxylato complexes and the type of carboxylate coordination. *Coord. Chem. Rev.* **1980**, *33*, 227–250. [CrossRef]
46. Rudbari, H.A.; Saadati, A.; Aryaeifar, M.; Correia, I.; Marques, F.; Blacque, O.; Micale, N. Cytotoxic oxidovanadium(IV) complexes of tridentate halogen-substituted Schiff bases: First dinuclear V(IV) complexes with O $\rightarrow$ V^{IV} = O $\rightarrow$ V^{IV} = O core. *Bioorg. Med. Chem. Lett.* **2021**, *49*, 128285. [CrossRef] [PubMed]
47. Hamilton, D.E. Reinvestigation of the vanadium-oxygen stretch in the IR spectrum of bis[N-(4-chlorophenyl)salicylideneiminato] oxovanadium(IV). *Inorg. Chem.* **1991**, *30*, 1670–1671. [CrossRef]
48. Sakiyama, H.; Abiko, T.; Yoshida, K.; Shomura, K.; Mitsuhashi, R.; Koyama, Y.; Mikuriya, M.; Koikawa, M.; Mitsumi, M. Detailed magnetic analysis and successful deep-neural-network-based conformational prediction for $[VO(dmso)_5][BPh_4]_2$. *RSC Adv.* **2020**, *10*, 9678–9685. [CrossRef] [PubMed]
49. O'Connor, C.J. Magnetochemistry–Advances in theory and experimentation. In *Progress in Inorganic Chemistry*; Lippard, S.J., Ed.; John Wiley & Sons: New York, NY, USA, 1982; Volume 29, pp. 203–283. [CrossRef]
50. Chilton, N.F.; Anderson, R.P.; Turner, L.D.; Soncini, A.; Murray, K.S. PHI: A powerful new program for the analysis of anisotropic monomeric and exchange-coupled polynuclear *d*- and *f*-block complexes. *J. Comput. Chem.* **2013**, *34*, 1164–1175. [CrossRef]

Disclaimer/Publisher's Note: The statements, opinions and data contained in all publications are solely those of the individual author(s) and contributor(s) and not of MDPI and/or the editor(s). MDPI and/or the editor(s) disclaim responsibility for any injury to people or property resulting from any ideas, methods, instructions or products referred to in the content.